PHYSICAL REVIEW RESEARCH **4**, 013066 (2022)

Electron-rotation coupling in UV photodissociation of aligned diatomics

Yan Rong Liu,[1] Victor Kimberg,[2,3] Yong Wu,[4,5] Jian Guo Wang,[4] Oriol Vendrell,[6] and Song Bin Zhang[1,*]
[1]*School of Physics and Information Technology, Shaanxi Normal University, Xi'an 710119, China*
[2]*Theoretical Chemistry and Biology, Royal Institute of Technology, Stockholm 10691, Sweden*
[3]*International Research Center of Spectroscopy and Quantum Chemistry, Siberian Federal University – IRC SQC,*
660041 Krasnoyarsk, Russia
[4]*Institute of Applied Physics and Computational Mathematics, Beijing 100088, China*
[5]*Center for Applied Physics and Technology, Peking University, Beijing 100084, China*
[6]*Theoretical Chemistry, Institute of Physical Chemistry, Heidelberg University, 69120 Heidelberg, Germany*

(Received 22 October 2021; accepted 4 January 2022; published 31 January 2022)

We investigate the effect of electron-rotation coupling ($\mathbf{R}-\Omega$ coupling) on fs UV photodissociation dynamics of aligned diatomic molecules. We consider the showcase of ground-state MgH$^+$ ($^1\Sigma^+$) pumped by an fs IR pulse, which initiates rotational dynamics leading to field-free molecular alignment. A time-delayed fs UV pulse probes the degree of alignment of the rotational wave packet in the framework of photodissociation spectroscopy. The molecular alignment correlates directly with the angular distribution of the photofragments in the dissociative $^1\Pi$ state, as it is shown in our simulations comparing the cases when the $\mathbf{R}-\Omega$ coupling is included and ignored. We show how the angular distribution of the photofragment is strongly affected by the $\mathbf{R}-\Omega$ coupling at various delay times with specific molecular alignment. It was shown that increases of the fs UV pulse intensity and the degree of alignment enhance the effect of $\mathbf{R}-\Omega$ coupling on the angular distribution of the photofragments. On the contrary, an increase of the initial temperature tends to reduce the effect of $\mathbf{R}-\Omega$ coupling, which is explained by the fact that such an effect turns smaller as the increasing of magnetic state $|\mathrm{M}_0|$ for each initial rotational state J_0; furthermore, higher excited rotational state J_0 contains more magnetic states M_0, and the results have been averaged over all degenerated M_0 states.

DOI: 10.1103/PhysRevResearch.4.013066

I. INTRODUCTION

With the development of ultrashort intense laser sources, numerous light-induced ultrafast nonlinear processes in atoms and molecules have been revealed and investigated, such as field-free molecular alignment and orientation [1–4], high harmonic generation [5–10], light-induced conical intersection [11–13], above threshold dissociation [14–16], and so on. The pump-probe technique provides versatile schemes to imprint these ultrafast dynamics. For example, when the system is pumped by ultrashort intense IR pulses, a special rotational wave packet leading to field-free molecular alignment can be generated [1]. These dynamics can be traced with the help of probe pulses, allowing for manipulation of photodissociation production [17–19], the study of ionization under strong field laser [20–22], and for control of the high harmonic generation [23–25].

As a fundamental case of light-induced ultrafast nuclear dynamics, photodissociation by ultrashort intense pulses have attracted a broad interest in the past years [26–31]. It was applied for control of electron excitation and localization in the dissociation of H$_2^+$ and its isotopes using two sequential ultrashort laser pulses [32], analyzing photodissociation of ultracold diatomic strontium molecules with quantum state control [33], controlling fragment spatial distributions from a photodissociation reaction with strong laser field [34], analyzing oscillation of branching ratios between the D(2s) + D(1s) and the D(2p) +D(1s) channels in direct photodissociation of D$_2$ [35], and exploring angle-resolved Rabi flopping in strong-field dissociation [36] to mention few. In a series of recent works it was shown that the effect of $\mathbf{R}-\Omega$ coupling affects strongly photodissociation dynamics in intense laser fields on its angular distributions of photofragments [37–40], which stresses a fundamental interest in accurate modeling of those processes in strong laser fields for a robust prediction of experimental outcome.

In the electronic states of diatomics with nonzero projection of total electronic angular momentum onto its interatomic axis as Ω, it intrinsically couples to the rotational angular momentum $\mathbf{R}$ as the total angular momentum $\mathbf{J}$. For the electronic transitions between Σ and Π states, $\mathbf{R}-\Omega$ coupling is naturally involved. In the case of interaction with intense resonant pulses, the effect of $\mathbf{R}-\Omega$ coupling plays an important role on observables directly related to the rotational dynamics in photoexcitation and photodissociation processes [37,38]. As we have shown earlier, in the case of interaction with an

---

[*] song-bin.zhang@snnu.edu.cn

intense x-ray pulse, this effect is greatly suppressed due to the presence of the fast Auger decay channel [39]. In order to increase feasibility of the experimental observation of the $\mathbf{R}-\Omega$ coupling effect, a versatile UV pump-probe photodissociation scheme has been proposed where excitation of a bound-bound transition is followed by a photodissociation at the second step by a time-delayed probe pulse [40].

In these previous studies, however, initial isotropic molecular ensemble at zero temperature was assumed in the simulations. In the present paper we address some questions of a general interest: How does the $\mathbf{R}-\Omega$ coupling effect manifest in the case of prealigned molecular ensemble? Would it appear more significantly or less significantly in the angular distribution of photofragments (ADPs) for the prealigned molecules? How would the temperature affect the effect? Here we answer those questions with the help of a theoretical IR-pump–UV-probe scheme and reveal that the $\mathbf{R}-\Omega$ coupling indeed shows a stronger effect for the prealigned molecules.

We consider a field-free prealigned MgH^+ molecular ensemble as a showcase in its ground electronic state $^1\Sigma^+$ created by an ultrashort intense IR-pump pulse. Note that MgH^+ is a typical system with a well-isolated dissociative Π state studied by many groups [41,43–45]; its $^1\Sigma^+ -^1\Pi$ transition is a very good candidate to reveal the $\mathbf{R}-\Omega$ coupling effect [37,38]. In the proposed scheme, a fs IR-pump pulse first creates rotational excitations. The system is then probed with a time-delayed resonant fs UV pulse, which leads to the photodissociation in $^1\Pi$ state. We study the effect of $\mathbf{R}-\Omega$ coupling in ADPs with variations of the probe pulse intensity and the time delay in respect to the pump pulse, which corresponds to different degrees of alignment.

The paper is organized as follows: Theoretical treatments of IR-pump–UV-probe scheme for MgH^+ as a showcase are briefly introduced in Sec. II; Sec. III is devoted to the discussions of molecular alignment, density of rotational wave packet, and ADPs. Conclusions of the present work are given in Sec. IV. Atomic units (a.u.) are used through the whole paper if otherwise not stated explicitly.

II. COMPUTATIONAL METHODS

The proposed IR-pump–UV-probe scheme is illustrated in Fig. 1(a); potential energy curves (PECs), dipole moments, and polarizabilities of MgH^+ are shown in Figs. 1(b) and 1(c), respectively. The nonresonant IR-pump pulse with a wavelength of 1000 nm ($\omega_1 = 1.24$ eV) triggers rotational dynamics and molecular alignment in the ground electronic state $^1\Sigma^+$ by Raman-type transitions. The time-delayed UV-probe pulse with $\omega_2 = 6.56$ eV promotes molecule from the ground-state $^1\Sigma^+$ to the dissociative excited state $^1\Pi$. Both pulses are supposed to have linear polarization along the Z axis in space-fixed (SF) frame and Gaussian envelope with pulse duration of 50 fs.

The time-dependent nuclear dynamic equation involving states $^1\Sigma^+$ and $^1\Pi$ can be written as

$$i\frac{\partial}{\partial t}[\Phi_\Sigma,\Phi_\Pi]^{\mathrm{T}} = \mathbf{H}(\mathbf{q},t)[\Phi_\Sigma,\Phi_\Pi]^{\mathrm{T}}, \tag{1}$$

where Φ_Σ and Φ_Π are the nuclear wave packets on states $^1\Sigma^+$ and $^1\Pi$, respectively. The corresponding nuclear Hamiltonian $\mathbf{H}(\mathbf{q},t)$ for the system can be written as

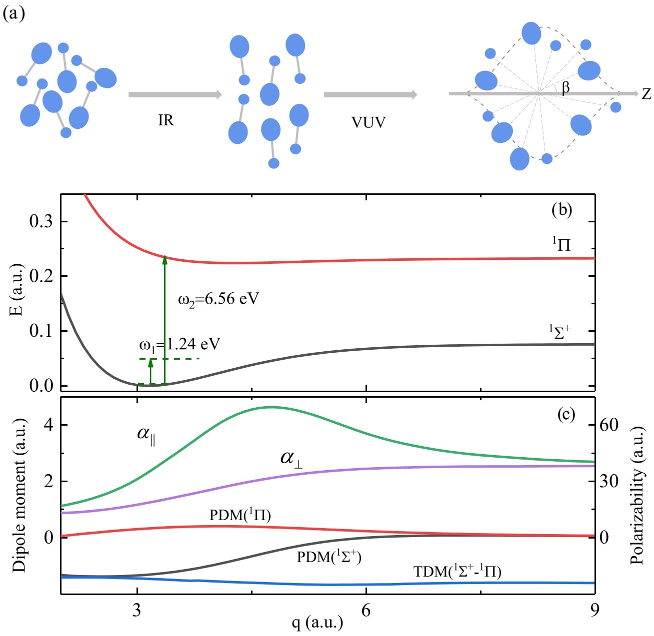

FIG. 1. (a) Illustration of the dissociative IR-pump–UV-probe scheme for diatomics; (b) PECs of MgH^+ for $^1\Sigma^+$ and $^1\Pi$ electronic states; (c) the PDM, and TDMs for the states involved (data are reproduced from Ref. [41]). The parallel $\alpha_\parallel$ and perpendicular $\alpha_\perp$ components of the dipole polarizability of the ground state (data are reproduced from Ref. [42]). The IR-pump pulse ($\omega_1 = 1.24$ eV) triggers ground-state $^1\Sigma^+$ alignment dynamics which are resonantly probed by time-delayed UV pulses ($\omega_2 = 6.56$ eV) in the framework of the photodissociation spectroscopy of $^1\Pi$ state.

$$\mathbf{H}(\mathbf{q},t) = \left(-\frac{1}{2m_\mu}\frac{\partial^2}{\partial \mathrm{q}^2} + \frac{\mathbf{R}^2}{2m_\mu \mathrm{q}^2}\right) + \begin{pmatrix} \mathrm{V}_\Sigma(\mathrm{q}) & 0 \\ 0 & \mathrm{V}_\Pi(\mathrm{q}) \end{pmatrix} + \begin{pmatrix} \mathrm{T}^1_\Sigma + \mathrm{T}^2_\Sigma & \left(\mathrm{T}^2_{\Sigma-\Pi}\right)^\dagger \\ \mathrm{T}^2_{\Sigma-\Pi} & \mathrm{T}^2_\Pi \end{pmatrix}, \tag{2}$$

where the first term includes the vibrational and rotational kinetic operators, m_μ is the reduced mass of MgH^+, and q is the internuclear distance. $\mathbf{R}$ is the nuclear rotational angular momentum, and $\mathbf{R}^2 = \mathbf{J}^2 - \Omega^2$ with $\mathbf{J}$ and $\Omega = \Lambda + \Sigma$ are the total angular momentum and the total interior angular momentum about the molecular-fixed (MF) z axis, respectively, and Λ and Σ are the projections of the total orbital $\mathbf{L}$ and spin $\mathbf{S}$ angular moment onto the MF z axis [46]. In the second term, $\mathrm{V}_\Sigma(\mathrm{q})$ and $\mathrm{V}_\Pi(\mathrm{q})$ correspond to the PECs of states $^1\Sigma^+$ and $^1\Pi$, respectively.

The laser–molecule interaction is described in the third term of Eq. (2), where $\mathrm{T}^1_\Sigma = -\mu_\Sigma(\mathrm{q})\varepsilon_1(\omega_1,t_1)\cos\beta - \frac{1}{2}\Delta\alpha(\mathrm{q})\varepsilon_1^2(\omega_1,t_1)\cos^2\beta$ describes rotational dynamics and alignments in the ground state triggered by the IR-pump pulse; $\mathrm{T}^2_\Sigma = -\mu_\Sigma(\mathrm{q})\varepsilon_2(\omega_2,t_2)\cos\beta$ and $\mathrm{T}^2_\Pi = -\mu_\Pi(\mathrm{q})\varepsilon_2(\omega_2,t_2)\cos\beta$ represent the permanent dipole interactions with UV-probe pulse in the ground and excited states, respectively; $\mu_\Sigma(\mathrm{q})$ and $\mu_\Pi(\mathrm{q})$ are the permanent dipole moments (PDMs) of electronic states $^1\Sigma^+$ and $^1\Pi$, respectively; $\Delta\alpha = \alpha_\parallel - \alpha_\perp$ is the difference between the parallel and the perpendicular components of the dipole polarizability of ground-state MgH$^+$, taken from Ref. [42]; $\varepsilon_1(\omega_1, \mathrm{t}_1)$ and $\varepsilon_2(\omega_2, \mathrm{t}_2)$ are the electric field of the IR-pump and UV-probe pulses, respectively, with time-delay $\Delta \mathrm{t} = \mathrm{t}_2 - \mathrm{t}_1$.

The transition operator from $^1\Sigma^+$ to $^1\Pi$ can be written as $\mathrm{T}^2_{\Sigma-\Pi} = \mu_{\Sigma-\Pi}(q)\varepsilon_2(\omega_2, t_2)\kappa_{\Sigma-\Pi}(\beta\gamma)$, where $\mu_{\Sigma-\Pi}(q)$ is the transition dipole moment (TDM); theory involving $\mathbf{R}-\Omega$ coupling requires $\kappa_{\Sigma-\Pi}(\beta\gamma) = \sin\beta\, e^{i\gamma}/\sqrt{2}$, yet theory neglecting $\mathbf{R}-\Omega$ coupling takes $\kappa_{\Sigma-\Pi}(\beta\gamma) = \sin\beta/\sqrt{2}$ [37,38], where β is the Euler angle between the MF z axis and the SF Z axis, and γ is the Euler angle representing rotations around the MF z axis [47]. Note that in the full theory with $\mathbf{R}-\Omega$ coupling, one-photon transition follows the exact selection rule as $\Delta\mathrm{J} = \pm 1$, while the conventional theory ignoring $\mathbf{R}-\Omega$ coupling relaxes the selection of J as $\Delta\mathrm{J} = 0, \pm 2, \pm 4, \ldots$.

After the IR-pump pulse, the degree of field-free molecular alignment in the ground-state $^1\Sigma^+$ can be described as $\langle\cos^2\beta\rangle_\Sigma(t) = \langle\Phi_\Sigma(t)|\cos^2\beta|\Phi_\Sigma(t)\rangle$. The dissociation in the excited state triggered by the time-delayed UV-probe pulse can be computed using complex absorbing potential (CAP) technique in the form of $-i W(\mathrm{q}) = -i\eta(\mathrm{q} - \mathrm{q_c})^3\Theta(\mathrm{q} - \mathrm{q_c})$, where η is the CAP strength, $\mathrm{q_c}$ is the point where the CAP is switched on, and Θ is Heaviside's step function [48,49]. The angular distribution of photofragments (ADP) at the excited dissociative state $^1\Pi$ is computed as

$$P^{\Pi}_{\mathrm{angle}}(\beta_j) = \frac{1}{w_j}\int_0^\infty \langle\Phi_\Pi(t)|W_{\beta_j}|\Phi_\Pi(t)\rangle \mathrm{d}t, \qquad (3)$$

where w_j is the weight factor corresponding to relevant grid point in the applied discrete variable representation (DVR) basis, W_{β_j} is the projection of the CAP onto a specific grid point associated with rotational degree of freedom (DOF) [48,49].

For the thermal equilibrium ensemble in the ground electronic state with initial rotational temperature T_0, the thermally averaged physical quantity O can be calculated as $\mathrm{O} = \sum_{\mathrm{J_0M_0}} w_{\mathrm{J_0M_0}}\mathrm{O}_{\mathrm{J_0M_0}}$, where $\mathrm{O}_{\mathrm{J_0M_0}}$ represents the physical quantity (such as molecular alignment, density of rotational wave packet, and ADPs) for a given initial angular state $\mathrm{J_0M_0}$, with $\mathrm{M_0}$ being the magnetic state and the projection of rotational state $\mathrm{J_0}$ onto the SF Z axis. The contribution of the physical quantity O from a specific initial rotational state $\mathrm{J_0}$ is represented as $\mathrm{O}_{\mathrm{J_0}} = \sum_{\mathrm{M_0}} w_{\mathrm{J_0M_0}}\mathrm{O}_{\mathrm{J_0M_0}}$. For heteronuclear diatomics $w_{\mathrm{J_0M_0}} = \frac{e^{-\mathrm{E_{J_0}}/k_B\mathrm{T_0}}}{\sum_{\mathrm{J_0}}(2\mathrm{J_0}+1)e^{-\mathrm{E_{J_0}}/k_B\mathrm{T_0}}}$ are the statistical weights according to a Boltzmann distribution of the rotational DOF; $\mathrm{E_{J_0}}$ is the rotational energy; k_B is the Boltzman constant [50].

The simulations were performed with the Heidelberg MCTDH package [49,51]. The vibrational DOF q is described by 281 sin-DVRs equally distributed in the region of [2.0–30.0] a.u.; 101 basis functions have been used for the rotational DOF β by Legendre polynomials when neglecting $\mathbf{R}-\Omega$ coupling and $\mathrm{L_2}$-normalized Wigner D functions when involving $\mathbf{R}-\Omega$ coupling, 11 and 5 exp-DVR for γ and α, respectively. The number of single particle functions for both DOF on the two electronic states was 20. The CAP is applied with $\eta = 3 \times 10^{-5}$ a.u. and $\mathrm{q_c} = 20$ a.u. The pulse is applied as $\varepsilon_i(\omega_i, t_i) = \mathrm{g_{i0}g_i(t)\cos(\omega_i t_i)}$ with intensity g_{i0} and Gaussian envelope $\mathrm{g_i(t)} = \exp(-\mathrm{t}^2/\tau^2)$ with $\tau = 50$ fs.

III. RESULTS AND DISCUSSIONS

Let us first focus on the case of initial zero rotational temperature or $\mathrm{J_0} = 0$. Figure 2(a) shows the evolution of the degree of molecular alignment $\langle\cos^2\beta\rangle_\Sigma(t)$ of the molecule in the ground-state $^1\Sigma^+$ induced by the nonresonant IR-pump pulse with peak intensity 10^{13} W/cm^2. The function $\langle\cos^2\beta\rangle_\Sigma(t)$ shows time-dependent periodical structures resulting from the coherent revival dynamics of the excited even J states triggered by the nonresonant pump pulse. The rotational wave packet at time $\mathrm{t_{M1}}$ reads $\Phi_{\mathrm{M1}} = \sum_{\mathrm{J}} \mathrm{C_J}|\mathrm{J}, 0, 0\rangle$. After the pulse, the time evolution of the rotational wave packet is described as $\Phi(t) = \sum_{\mathrm{J}} \mathrm{C_J}|\mathrm{J}, 0, 0\rangle e^{-i\mathrm{E_J t}}$, where $\mathrm{E_J}$ is the energy of a rotational level and t is the time delay relative to the moment $\mathrm{t_{M1}}$. Table I presents the coefficients of rotational state $\mathrm{C_J} = \mathrm{c_J}e^{i\theta_{\mathrm{J}}}$ at the moment $\mathrm{t_{M1}}$=586 fs (relative to peak envelope of IR-pump pulse), $\mathrm{c_J}$ is the amplitude of the rotational state J, and θ_{J} is the relative phase between $\mathrm{J} = 0$ and the other J state. Rotational state $\mathrm{J} = 2$ is excited by Raman-type transitions from the initial state $\mathrm{J_0} = 0$ in the $^1\Sigma^+$ electronic state, while other even rotational states can be excited in a ladder way. According to Table I, rotational level $\mathrm{J} = 0$, 2, 4, and 6 accumulate about 99.99% of rotational population; therefore these four J states are considered in the following analysis. Note that the $\mathbf{R}$-Ω coupling has been decoupled for the electronic state with $\Omega = 0$; such a coupling does not hold in the Raman process of ground electronic state $^1\Sigma^+$.

In order to study the relation between the degree of molecular alignment and the following photodissociation dynamics, let us consider three typical states of the molecular ensemble within one rotational period (see Fig. 2): (1) Cases with maximal values of degree of molecular alignment ($\mathrm{t_{P1}}$, $\mathrm{t_{P2}}$, and $\mathrm{t_{P3}}$), (2) cases with minimal alignment values ($\mathrm{t_{V1}}$, $\mathrm{t_{V2}}$, and $\mathrm{t_{V3}}$), and (3) cases with alignment equal to 1/3 ($\mathrm{t_{M1}}$, $\mathrm{t_{M2}}$, $\mathrm{t_{M3}}$, $\mathrm{t_{M4}}$, $\mathrm{t_{M5}}$, and $\mathrm{t_{M6}}$) or "isotropic" alignment. The density of the rotational wave packet of these cases is presented as black lines in Figs. 2(b)–2(m), the blue line represents the initial isotropic rotational wave packet before the pump pulse. One can see that in the case of "isotropic" alignment ($\langle\cos^2\beta\rangle_\Sigma(t) = 1/3$, $\mathrm{t_M}$ moments) the density of rotational wave packet may have a rather different shape [see Figs. 2(b)–2(g)] while the shape of the wave packet at the times correspondent to the minimal [(Figs. 2(h)–2(j)] and maximal [Figs. 2(k)–2(m)] degrees of alignment shows rather similar distribution with peaks at $\beta = \pi/2$ and $\beta = 0, \pi$, respectively. The UV pulses at different time delays with respect to the pump-pulse probe the rotational dynamics in the framework of the photodissociation spectroscopy. The ADP spectra in the dissociative state $^1\Pi$ represent the effect of $\mathbf{R}$-Ω coupling, which is naturally involved in the $\Sigma - \Pi$ transitions.

Figure 3 shows ADP profiles for the case of degree of alignment reaching minimum values ($\mathrm{t_{V1}}$, $\mathrm{t_{V2}}$, and $\mathrm{t_{V3}}$) and maximum values ($\mathrm{t_{P1}}$, $\mathrm{t_{P2}}$, and $\mathrm{t_{P3}}$) for three different intensities of the probe field (10^{11} W/cm^2, 10^{12} W/cm^2, and 10^{13} W/cm^2). With an increase of the probe pulse intensity

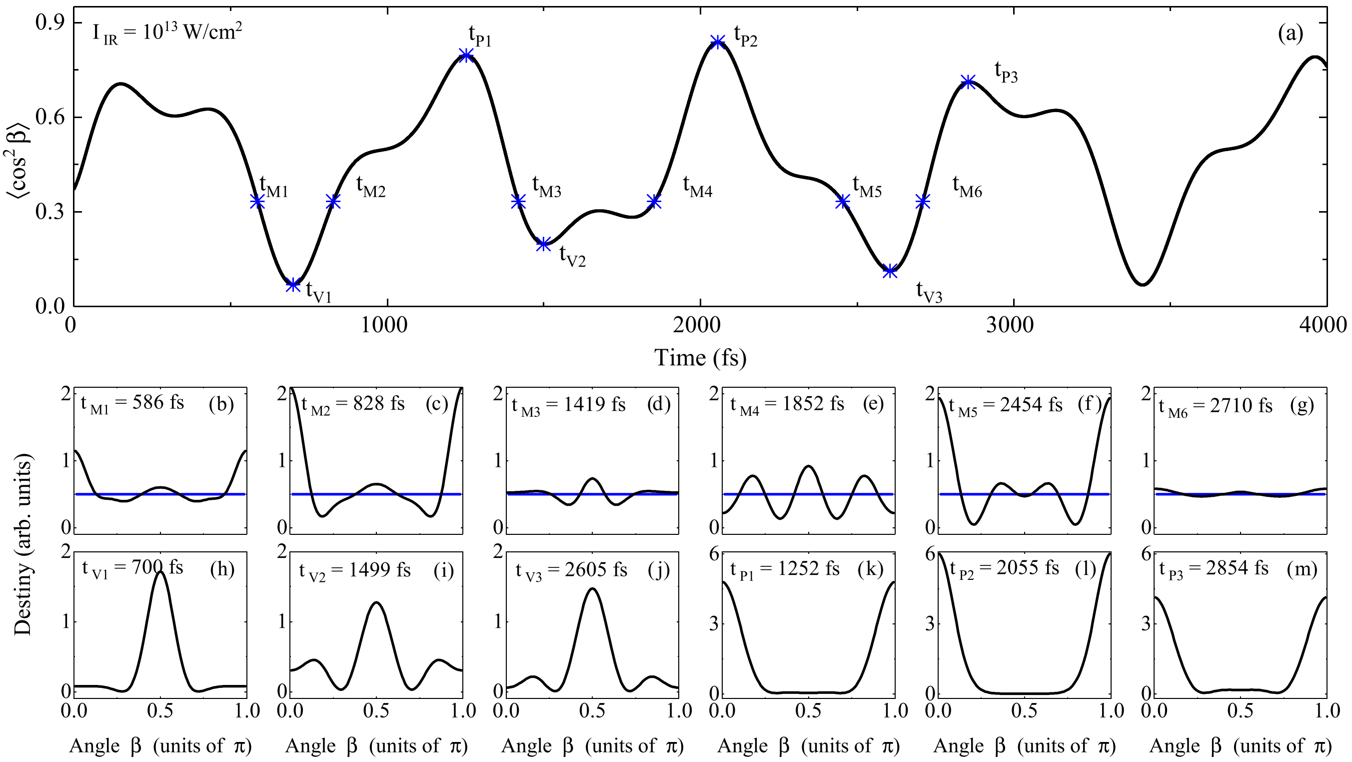

FIG. 2. (a) Degree of molecular alignment $\langle\cos^2\beta\rangle_\Sigma(t)$ in the electronic ground-state ${}^1\Sigma^+$ induced by the IR-pump pulse of intensity 10^{13} W/cm^2, and pump pulse is centered at $t_1 = 0$ fs; t_{P1}, t_{P2}, and t_{P3} are the moments with maximal degrees of alignment; t_{V1}, t_{V2}, and t_{V3} are the moments of alignment reach minimum value; and t_{M1}, t_{M2}, t_{M3}, t_{M4}, t_{M5}, and t_{M6} are the moments of alignment equals to 1/3 ("isotropic" cases of $\langle\cos^2\beta\rangle_\Sigma(t) = 1/3$). (b)–(m) Density of rotational wave packet at corresponding time (black lines), and density of rotational wave packet before the pump pulse (blue lines).

the effect of the **R**−Ω coupling becomes more pronounced for the angles $\beta < 0.25\pi$; related to the Rabi-flopping in intense probe field, similar features have been observed and comprehensively discussed in our previous work for isotropic molecular ensemble [37,38]. Figures 3(a)–3(c) show ADP profiles for the time delays correspondent to the small degree of alignment [see t_V moments in Fig. 2(a)]. In these moments the wave packet in the ground-state ${}^1\Sigma^+$ is mainly distributed near $\beta = 0.5\pi$ [Figs. 2(h)–2(j)]; therefore the angular distribution after dissociation in the excited ${}^1\Pi$ state has maximum near $\beta = 0.5\pi$. The effect of **R**−Ω coupling in ADP spectra is observed at small angles $\beta \leqslant 45^\circ$ and is not very significant. Figures 3(d)–3(f) show ADP profiles for the probe pulses centered at the times of maximal degree of alignment [see t_P moments in Fig. 2(a)] where the rotational wave packets are located mainly around $\beta = 0$ and $\beta = \pi$ [see Figs. 2(k)–2(m)]. Due to this the angular distribution after the dissociation is also located near $\beta = 0$ and $\beta = \pi$. The effect of the **R**−Ω coupling at small angles $\beta \leqslant 45^\circ$ is much stronger as in the case of the small degree of molecular alignment. It can be concluded that the larger degree of alignment results in greater influence of **R**−Ω coupling in ADP spectra.

TABLE I. Energies E_J and coefficients $C_J = c_J e^{i\theta_J}$ of rotational J states in electronic state ${}^1\Sigma^+$ at time t_{M1} [see Fig. 2(a)].

	J = 0	J = 2	J = 4	J = 6
E_J	0.00000000	0.00016837	0.00056079	0.00117620
c_J	0.60079374	0.73274781	0.31058467	0.07440619
θ_J	0.00000000	4.13620535	2.68425630	2.19541563

The ADP spectra is affected through both the density of rotational wave packet at the delay time of the probe pulse and the dynamics photodissociation process in strong UV fields. In order to understand the ADP spectra, let us ignore strong field effects and analyze one-photon transitions at the weak probe field. For aligned molecules, the rotational state can be described as $|J, M, \Omega\rangle$ when **R**-Ω coupling is included and $|J, M\rangle$ when the coupling is neglected. For the excitation from the ${}^1\Sigma^+$ to ${}^1\Pi$ state the transition matrix elements are $\langle J', M', \Omega'|\sin\beta\, e^{i\gamma}/\sqrt{2}|J, M, \Omega\rangle$ (with **R**-Ω coupling) and $\langle J', M'|\sin\beta/\sqrt{2}|J, M\rangle$ (neglecting **R**-Ω coupling); the matrix elements are conserved for the electronic transition and relaxes the selection, respectively [40]. The rotational wave packet in the dissociated state is expressed as $\Phi' = \sum_{J'}\sum_{J}\langle J', 0, 1|\sin\beta\, e^{i\gamma}/\sqrt{2}|J, 0, 0\rangle C_J|J', 0, 1\rangle e^{-iE_Jt}$ for the case when **R**-Ω coupling is included with selection rule $J' = J \pm 1$. In the case when **R**-Ω coupling is neglected, the wave packet reads $\Phi' = \sum_{J'}\sum_{J}\langle J', 0|\sin\beta/\sqrt{2}|J, 0\rangle C_J|J', 0\rangle e^{-iE_Jt}$ and $J' = J \pm 0, \pm 2, \ldots$. The density of rotational wave-packet Φ' can be used for a simplified understanding of the ADP spectra (Fig. 3) for the weak probe field.

Figure 4 shows ADP profiles probed at the moments of "isotropic" alignment ($\langle\cos^2\beta\rangle_\Sigma(t) = 1/3$) $t_{M1} - t_{M6}$ for various probe pulse intensities (10^{11} W/cm^2, 10^{12} W/cm^2,

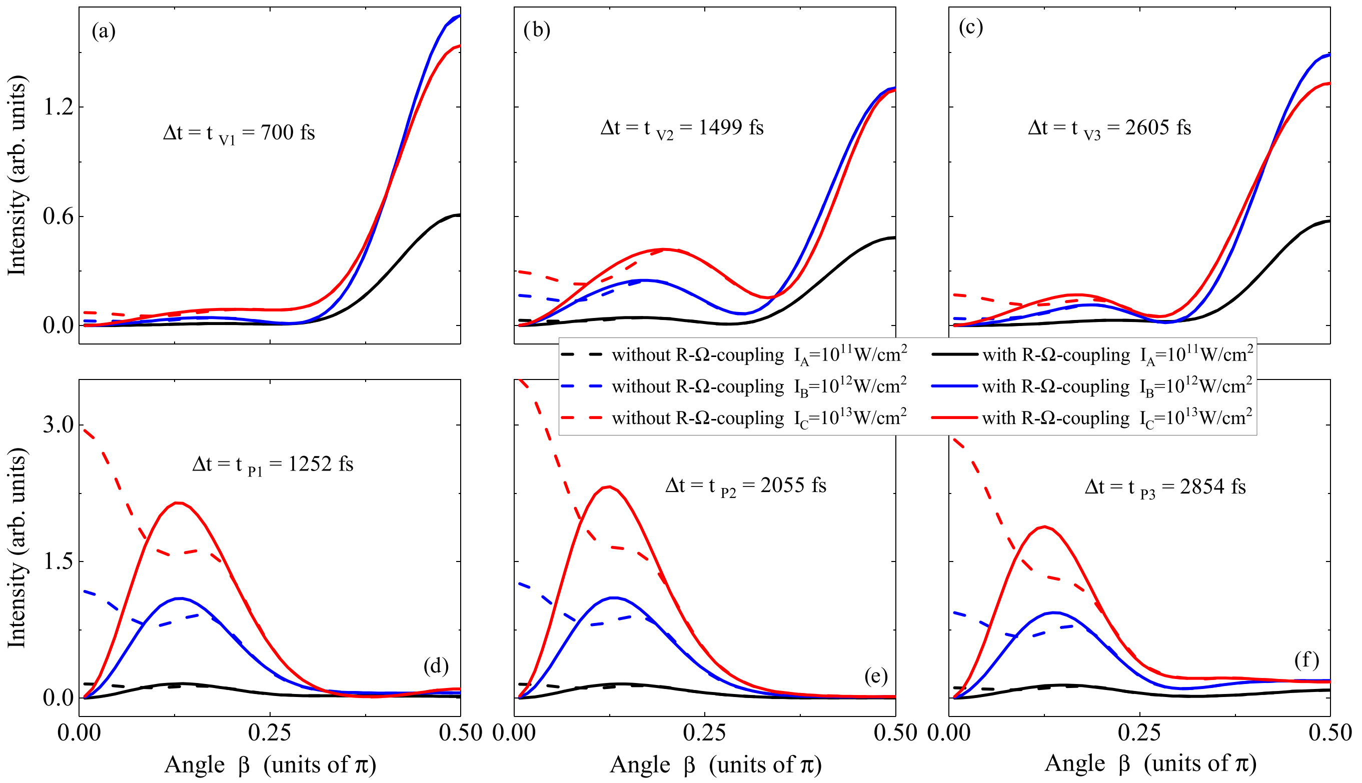

FIG. 3. ADP in the dissociative state $^1\Pi$ for the probe pulse centered at the moments correspondent to the minimum values t_{V1}, t_{V2}, and t_{V3} and maximum values t_{P1}, t_{P2}, and t_{P3} of molecular alignment. The probe pulse intensities are 10^{11} W/cm^2(black lines), 10^{12} W/cm^2(blue lines), and 10^{13} W/cm^2(red lines). Simulations compare theory with and without $\mathbf{R}-\Omega$ coupling, shown by solid lines and dashed lines, respectively.

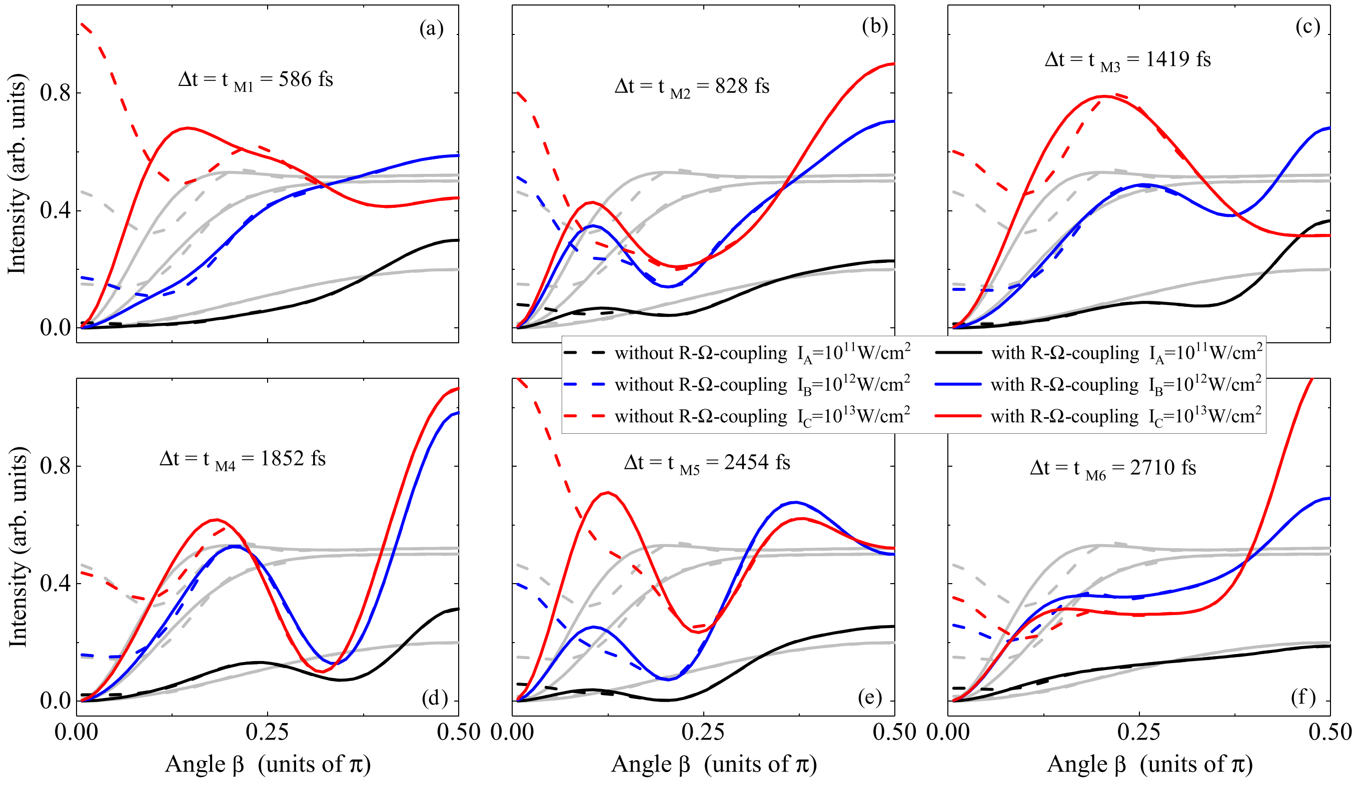

FIG. 4. ADP profiles in the dissociative state $^1\Pi$ for the moments $t_{M1} - t_{M6}$ with "isotropic" molecular alignment. All notations and pulse parameters are the same as in Fig. 4; gray lines show the ADP without pump pulse.

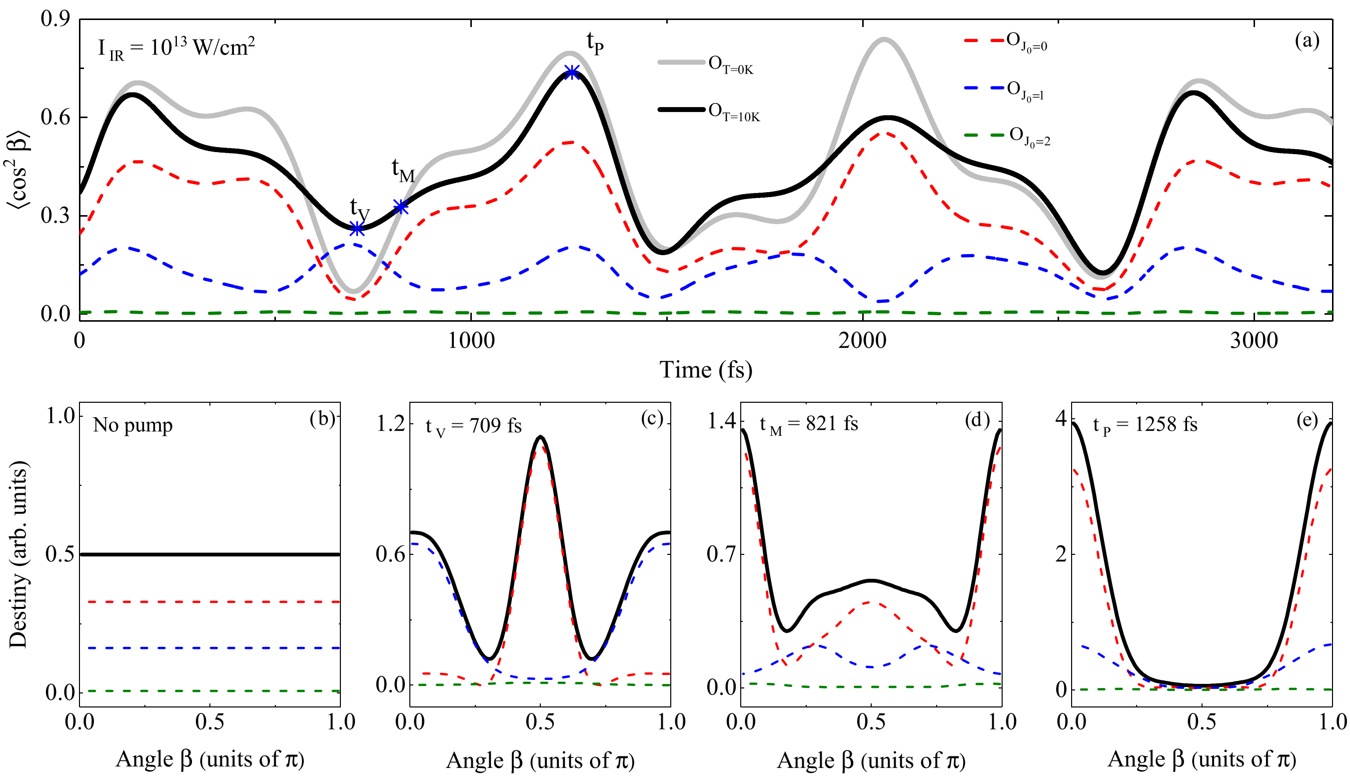

FIG. 5. Degree of molecular alignment (a) at initial rotational temperature $\mathrm{T} = 10$ K (black lines) and $\mathrm{T} = 0$ K (gray lines); $\mathrm{t_V}$, $\mathrm{t_M}$, and $\mathrm{t_P}$ moments correspond to the moments when alignment is minimum, 1/3 ("isotropic"), and maximum, respectively. IR-pump-pulse intensity is $10^{13}\ \mathrm{W/cm^2}$ and the pulse is centered at $\mathrm{t} = 0$ fs. The density of rotational wave packet without the pump pulse (b) and at moments $\mathrm{t_V}$, $\mathrm{t_M}$, and $\mathrm{t_P}$ (c)–(e), respectively. The dashed red, blue, and green lines correspond to the contribution from $\mathrm{J_0} = 0$, $\mathrm{J_0} = 1$, and $\mathrm{J_0} = 2$ at $\mathrm{T} = 10$ K, respectively [plots (a–e)].

and $10^{13}\ \mathrm{W/cm^2}$); gray lines are the ADP spectra probed at the initial isotropic case (without pump pulse). The $\mathbf{R}-\Omega$ coupling effect is significant for the small angles $\beta \leqslant 45^\circ$ at any intensities. It is worthwhile to note that ADP is zero at $\beta = 0$ when $\mathbf{R}-\Omega$ coupling is included, while it becomes large without $\mathbf{R}-\Omega$ coupling, which shows great importance. The difference in ADP caused by $\mathbf{R}-\Omega$ coupling grows with the increase of pulse intensity in a similar way as it was discussed before for Fig. 4. One can see considerable variation of the ADP profile for different delay times even though they correspond to the same degree of alignment of 1/3 [Figs. 4(a)–4(f)], which is explained by sufficient difference of the shape of the rotational wave packet at these moments [see Figs. 2(b)–2(g)].

Let us now consider the case when initial rotational temperature is set to $\mathrm{T} = 10$ K. Now physical quantities O (molecular alignment, density of rotational wave packet, and ADPs) are calculated with statistical weights $w_{\mathrm{J_0=0M_0}} = 0.6592$, $w_{\mathrm{J_0=1M_0}} = 0.3260$, and $w_{\mathrm{J_0=2M_0}} = 0.0148$. Figure 5(a) compares evolution of degree of molecular alignment in the ground-state ${}^1\Sigma^+$ at initial rotational temperature $\mathrm{T} = 10$ K (black line) and $\mathrm{T} = 0$ K (gray line). Obviously lower initial rotational temperature of the molecular ensemble results in a higher degree of molecular alignment in general, consistent with Ref. [1], except for the cases of nonequilibrium distribution when contribution from the higher rotational states is large enough to show its own character. For further analysis, we choose three moments when the degree of molecular alignment reaches its minimum ($\mathrm{t_V}$), 1/3 ($\mathrm{t_M}$), and maximum ($\mathrm{t_P}$). The dashed lines in Fig. 5(a) illustrate the contribution from $\mathrm{J_0} = 0$ (red), $\mathrm{J_0} = 1$ (blue), and $\mathrm{J_0} = 2$ (green) initial rotational state at $\mathrm{T} = 10$ K. One can see that the main contribution is given from $\mathrm{J_0} = 0$ and $\mathrm{J_0} = 1$. Those contributions are principally different, e.g., they contribute constructively to increased degree of molecular alignment at moment $\mathrm{t_P}$, while they give opposite contribution at the moment $\mathrm{t_V}$. The density of rotational wave packet without pump pulse is presented in Fig. 5(b) and at moments $\mathrm{t_V}$, $\mathrm{t_M}$, and $\mathrm{t_P}$ are presented in Figs. 5(c)–5(e). The pump-free system shows isotropic density of rotational wave packet for any initial quantum number $\mathrm{J_0}$. For $\Delta t = t_{\mathrm{V}}$, $\mathrm{J_0} = 0$ gives a major contribution near $\beta = 0.5\pi$ and $\mathrm{J_0} = 1$ contributes mainly around $\beta = 0$ and $\beta = \pi$. For $\Delta t = t_{\mathrm{M}}$, the contribution from $\mathrm{J_0} = 0$ plays a major role in the formation of the angular distribution profile, except for $\beta = 0.25\pi$ and $\beta = 0.75\pi$, where $\mathrm{J_0} = 1$ gives sufficient contribution. For the moment of maximal degree of alignment, $\Delta t = t_{\mathrm{P}}$, the rotational wave packet is mainly distributed around $\beta = 0$ and $\beta = \pi$; the contribution from $\mathrm{J_0} = 0$ is almost five times larger at $\beta \approx 0$ as compared with the contribution from $\mathrm{J_0} = 1$.

Figure 6 shows ADP for the pump-free system (a) and various degrees of alignment; black lines and blue lines correspond to ADP at initial rotational temperature $\mathrm{T} = 10$ K and $\mathrm{T} = 0$ K; solid lines and dashed lines are ADP computed with

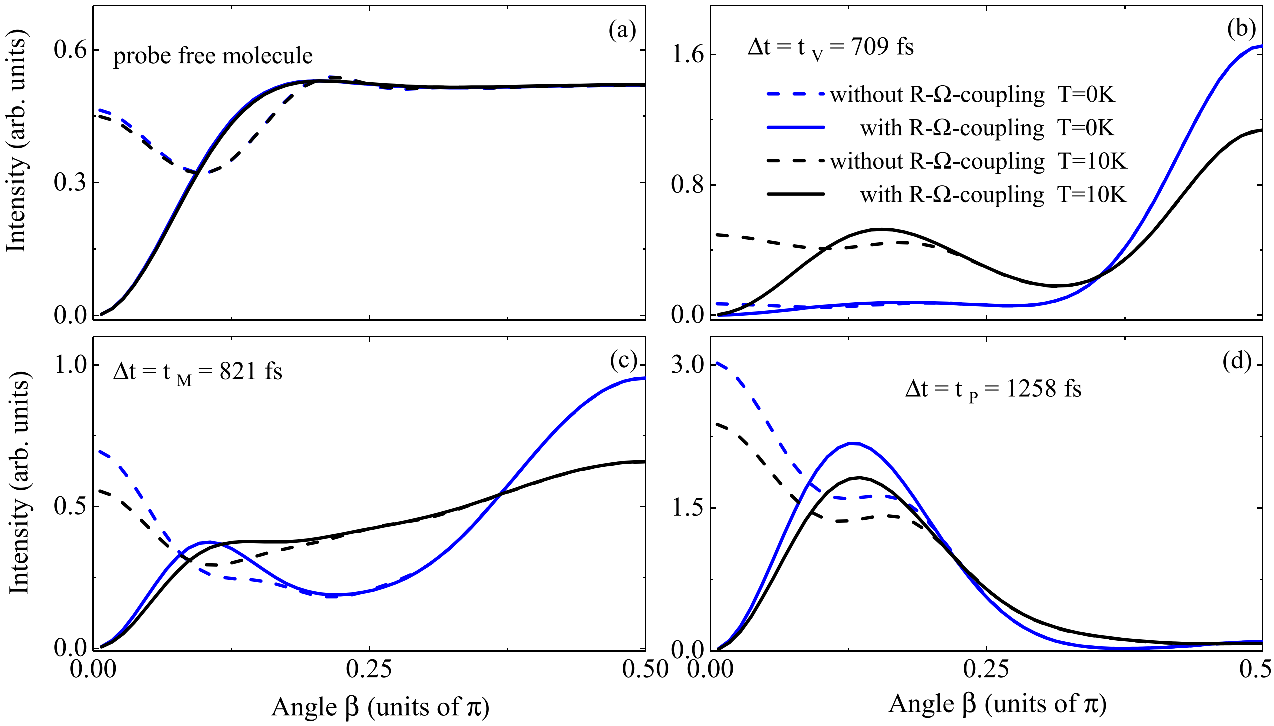

FIG. 6. ADP for the pump-free system (a) and various degrees of alignment: Minimal (b), “isotropic” (c), and maximal (d). Initial rotational temperature is T = 10 K (black lines) and T = 0 K (blue lines). The probe pulse intensity is 10^{13} W/cm^2. Simulations compare theory with and without $\mathbf{R}-\Omega$ coupling taken into account and are shown by solid and dashed lines, respectively.

and without $\mathbf{R}-\Omega$ coupling taken into account, respectively. For the case with no pump pulse, the initial rotational temperature has only a small effect on the angular distribution. The ADPs at T = 10 K and T = 0 K are almost the same for the calculations where $\mathbf{R}-\Omega$ coupling is included, and the ADP at T = 10 K is a little bit smaller than T = 0 K near $\beta = 0$ for the theory without $\mathbf{R}-\Omega$ coupling. For time delay $\Delta t = t_\mathrm{V}$, as the initial rotational temperature increases, a new peak is formed near $\beta = 0.5\pi$ and the angular distribution goes from being mostly around $\beta = 0.15\pi$. Moreover, the effect of $\mathbf{R}-\Omega$ coupling increases sufficiently at small angles due to the contribution from $\mathrm{J}_0 = 1$, as is evident from Fig. 5(c). For time delay $\Delta t = t_\mathrm{M}$, with increasing initial rotational temperature, the ADP profile increases around $\beta = 0.25\pi$ and shows a linear behavior for larger angles, consistent with Fig. 6(c). The absolute effect of $\mathbf{R}-\Omega$ coupling for “isotropic” ensemble is the smallest as compared with other degrees of alignment [plots (b) and (d)] and is located at angles $\beta < 0.25\pi$. For the case of highest degree of alignment (time delay $\Delta t = t_\mathrm{P}$) the ADP profile has maximum toward smaller angles, and the effects of $\mathbf{R}-\Omega$ coupling and initial rotational temperature are the strongest among other cases. These examples show that the temperature effect reduces the impact of $\mathbf{R}-\Omega$ coupling in general, except for cases when the higher rotational states give sufficient contribution to the rotational wave packet.

The origin of the temperature effect on $\mathbf{R}-\Omega$ coupling deserves a special comment. Figure 7(a) shows the evolution of degree of molecular alignment in the ground state for a specific initial rotational state $\mathrm{J}_0 = 0, 1, 2$ induced by the IR-pump pulse. P corresponds to the moment when all initial J_0 states show most similar molecular alignment, which is then probed by the UV pulse with intensity 10^{13} W/cm^2. The results of ADP for the cases with (solid lines) and without (dashed lines) $\mathbf{R}-\Omega$ coupling for the three lowest initial state $\mathrm{J}_0 = 0, 1, 2$ are shown in Fig. 7(b), confirming the decrease of the $\mathbf{R}-\Omega$ coupling effect with the increase of J_0. In fact, this is a result of averaging over an increasing number of degenerated magnetic states M_0 for higher rotational state J_0. Contributions from different $|\mathrm{M}_0|$ states for $\mathrm{J}_0 = 1$ and 2 are shown in panels (c) and (d), respectively. As one can see, the $\mathbf{R}-\Omega$ coupling effect decreases with an increasing of $|\mathrm{M}_0|$ for each J_0, so the total effect of $\mathbf{R}-\Omega$ coupling becomes smaller after averaging over all the initial degenerate M_0 states for a higher J_0 state, where a larger number of M_0 states contribute. Summarizing, an increase of magnetic $|\mathrm{M}_0|$ state for each initial rotational J_0 state tends to reduce the $\mathbf{R}-\Omega$ coupling effect; a higher initial temperature increases the number of J_0 states; the higher J_0 states include an increasing number of degenerated $-\mathrm{J}_0 \leqslant \mathrm{M}_0 \leqslant \mathrm{J}_0$ states, and their collective contributions result in the diminishing of the $\mathbf{R}-\Omega$ coupling effect.

IV. CONCLUSION

In conclusion, the $\mathbf{R}-\Omega$ coupling manifests itself strongly for aligned molecular ensemble compared with isotropic distribution. As a showcase, we consider photodissociation dynamics of aligned MgH^+ molecular ensemble aligned by nonresonant IR-pump pulse at the ground-state $^1\Sigma^+$ and then excited to dissociative state $^1\Pi$ by time-delayed resonant UV-probe pulse. Observation of the angular distribution of

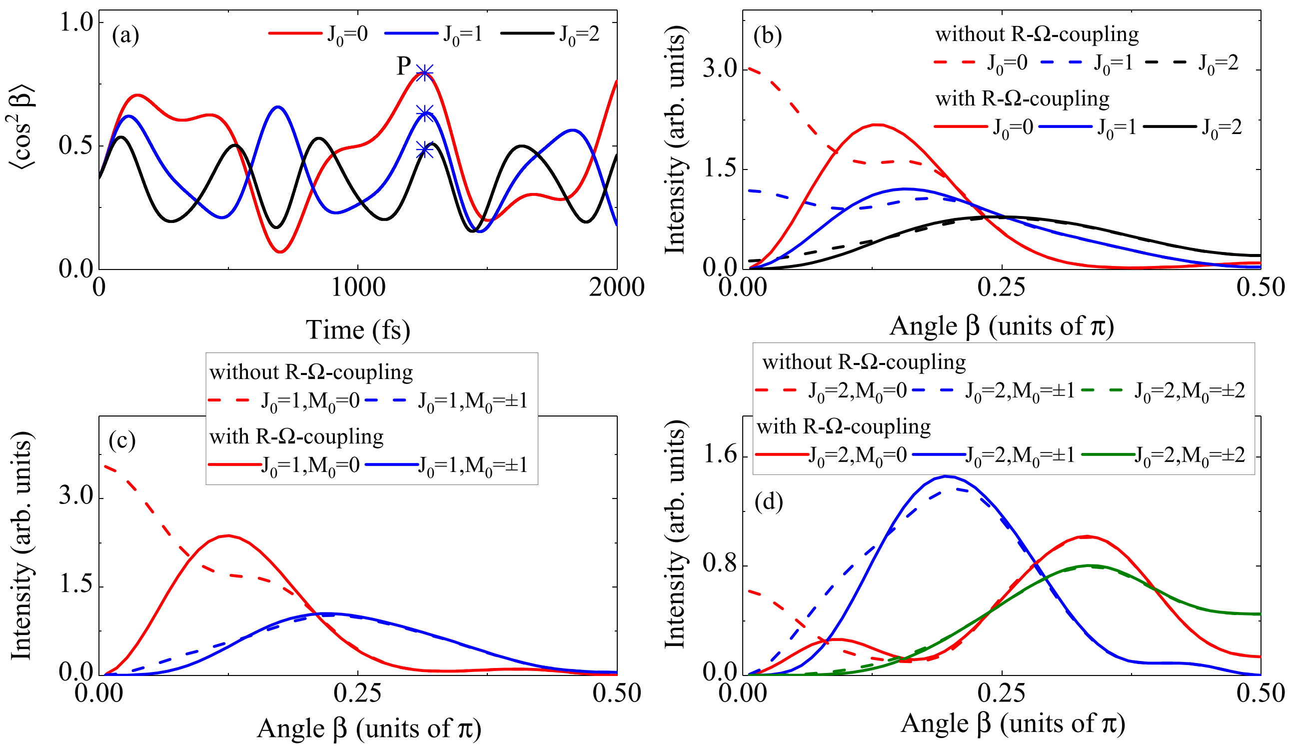

FIG. 7. (a) Degree of molecular alignment for initial rotational state $J_0 = 0, 1$, and 2 by IR-pump pulse with intensity 10^{13} W/cm^2 (centered at $t = 0$ fs). (b) ADP profiles in the dissociative state $^1\Pi$ originated from three initial states $J_0 = 0, 1, 2$ averaged over contributions from all magnetic M_0 states. (c, d) Partial ADPs for each M_0 states are shown for the case of $J_0 = 1$ (c) and $J_0 = 2$ (d). Our simulations in (b) and (c) compare the cases with (solid lines) and without (dashed lines) $\mathbf{R}-\Omega$ coupling taken into account. The rotational dynamics are probed at moment P [see (a)] with UV pulse intensity 10^{13} W/cm^2.

the photofragments allowed us to study the effects of $\mathbf{R}-\Omega$ coupling and initial rotational temperature. We study the ADP profiles at different delay times correspondent to different degrees of molecular alignment as well as for various intensities of the probe pulse. We show that stronger probe pulse intensity and larger degrees of alignment increase the influence of the $\mathbf{R}-\Omega$ coupling. In general, the effect of $\mathbf{R}-\Omega$ coupling is crucial at small angles ($\beta < 0.25\pi$) for $^1\Sigma^+ -^1\Pi$ transitions, where conventional theory neglecting the coupling effect gives incorrect predictions. We also show that probing the moments with the same degree of alignment may result in a rather different ADP profile due to different angular distribution of the initial wave packet. Analyzing the ADP with change of the initial rotational temperature, we have shown that an increase of the initial temperature tends to reduce the impact of $\mathbf{R}-\Omega$ coupling in general due to the averaging over all the degenerated initial magnetic states, except for the case when higher rotational state J_0 contributes sufficiently to the rotational wave packet. So, in order to make the $\mathbf{R}-\Omega$ coupling effect observable in the photodissociation spectroscopy experiment, we suggest to induce high degrees of alignment and to use cold targets for the measurements.

ACKNOWLEDGMENTS

Grants from NSFC (No. 11934004 and No. 11974230), the National Basic Research Program of China (2017YFA0403200), the National Key Research and Development Program of China (2020YFA0211300) are acknowledged. V.K. acknowledges financial support from the Russian Science Foundation (No. 21-12-00193) and the Swedish Research Council (No. 2019-03470).

---

[1] H. Stapelfeldt and T. Seideman, Colloquium: Aligning molecules with strong laser pulses, Rev. Mod. Phys. **75**, 543 (2003).

[2] O. Ghafur, A. Rouzée, A. Gijsbertsen, W. K. Siu, S. Stolte, and M. J. J. Vrakking, Impulsive orientation and alignment of quantum-state-selected NO molecules, Nat. Phys. **5**, 289 (2009).

[3] M. Spanner, S. Patchkovskii, E. Frumker, and P. Corkum, Mechanisms of Two-Color Laser-Induced Field-Free Molecular Orientation, Phys. Rev. Lett. **109**, 113001 (2012).

[4] K. Lin, I. Tutunnikov, J. Qiang, J. Ma, Q. Song, K. Lin, I. Tutunnikov, J. Qiang, J. Ma, Q. Song, Q. Ji, W. Zhang, H. Li, F. Sun, X. Gong, *et al.*, All-optical field-free three-dimensional orientation of asymmetric-top molecules, Nat. Commun. **9**, 5134 (2018).

[5] P. B. Corkum, Plasma Perspective on Strong Field Multiphoton Ionization, Phys. Rev. Lett. **71**, 1994 (1993).

[6] S. Kim, J. Jin, Y.-J. Kim, I.-Y. Park, Y. Kim, and S.-W. Kim, High-harmonic generation by resonant plasmon field enhancement, Nature (London) **453**, 757 (2008).

[7] H. J. Wörner, J. B. Bertrand, D. V. Kartashov, P. B. Corkum, and D. M. Villeneuve, Following a chemical reaction using high-harmonic interferometry, Nature (London) **466**, 604 (2010).

[8] J. Shao, C.-P. Zhang, J.-C. Jia, J.-L. Ma, and X.-Y. Miao, Effect of carrier envelope phase on high-order harmonic generation from solid, Chin. Phys. Lett. **36**, 054203 (2019).

[9] J. Zhang, L.-Q. Hua, Z. Chen, M.-F. Zhu, C. Gong, and X.-J. Liu, Extreme ultraviolet frequency comb with more than 100μ w average power below 100nm, Chin. Phys. Lett. **37**, 124203 (2020).

[10] H. Zhang, X. Liu, F. Jin, M. Zhu, S. Yang, W. Dong, X. Song, and W. Yang, Coherent control of high harmonic generation driven by metal nanotip photoemission, Chin. Phys. Lett. **38**, 063201 (2021).

[11] G. J. Halász, M. Šindelka, N. Moiseyev, L. S. Cederbaum, and A. Vibók, Light-induced conical intersections: Topological phase, wave packet dynamics, and molecular alignment, J. Phys. Chem. A **116**, 2636 (2012).

[12] P. V. Demekhin and L. S. Cederbaum, Light-induced conical intersections in polyatomic molecules: General theory, strategies of exploitation, and application, J. Chem. Phys. **139**, 154314 (2013).

[13] M. E. Corrales, J. González-Vázquez, G. Balerdi, I. R. Solá, R. de Nalda, and L. Bañares, Control of ultrafast molecular photodissociation by laser-field-induced potentials, Nat. Chem. **6**, 785 (2014).

[14] J. McKenna, A. M. Sayler, F. Anis, B. Gaire, N. G. Johnson, E. Parke, J. J. Hua, H. Mashiko, C. M. Nakamura, E. Moon, Z. Chang, K. D. Carnes, B. D. Esry, and I. Ben-Itzhak, Enhancing High-Order Above-Threshold Dissociation of H_2^+ Beams with Few-Cycle Laser Pulses, Phys. Rev. Lett. **100**, 133001 (2008).

[15] Q. Zhang, J. W. Hepburn, and M. Shapiro, Observation of above-threshold dissociation of ${Na_2}^+$ in intense laser fields, Phys. Rev. A **78**, 021403(R) (2008).

[16] P. Lu, J. Wang, H. Li, K. Lin, X. Gong, Q. Song, Q. Ji, W. Zhang, J. Ma, H. Li, *et al.*, High-order above-threshold dissociation of molecules, Proc. Natl. Acad. Sci. USA **115**, 2049 (2018).

[17] J. J. Larsen, I. Wendt-Larsen, and H. Stapelfeldt, Controlling the Branching Ratio of Photodissociation Using Aligned Molecules, Phys. Rev. Lett. **83**, 1123 (1999).

[18] P. Reckenthaeler, M. Centurion, W. Fuß, S. A. Trushin, F. Krausz, and E. E. Fill, Time-Resolved Electron Diffraction from Selectively Aligned Molecules, Phys. Rev. Lett. **102**, 213001 (2009).

[19] L. Z. Deng and J. P. Yin, Improved production of Br atoms near zero speed by photodissociating laser aligned Br_2 molecules, J. Chem. Phys. **141**, 164314 (2014).

[20] I. V. Litvinyuk, K. F. Lee, P. W. Dooley, D. M. Rayner, D. M. Villeneuve, and P. B. Corkum, Alignment-Dependent Strong Field Ionization of Molecules, Phys. Rev. Lett. **90**, 233003 (2003).

[21] D. Zeidler, A. Staudte, A. B. Bardon, D. M. Villeneuve, R. Dörner, and P. B. Corkum, Controlling Attosecond Double Ionization Dynamics Via Molecular Alignment, Phys. Rev. Lett. **95**, 203003 (2005).

[22] V. Kumarappan, L. Holmegaard, C. Martiny, C. B. Madsen, T. K. Kjeldsen, S. S. Viftrup, L. B. Madsen, and H. Stapelfeldt, Multiphoton Electron Angular Distributions from Laser-Aligned CS_2 Molecules, Phys. Rev. Lett. **100**, 093006 (2008).

[23] R. Velotta, N. Hay, M. B. Mason, M. Castillejo, and J. P. Marangos, High-Order Harmonic Generation in Aligned Molecules, Phys. Rev. Lett. **87**, 183901 (2001).

[24] J. Itatani, D. Zeidler, J. Levesque, M. Spanner, D. M. Villeneuve, and P. B. Corkum, Controlling High Harmonic Generation with Molecular Wave Packets, Phys. Rev. Lett. **94**, 123902 (2005).

[25] S. Ramakrishna and T. Seideman, Information Content of High Harmonics Generated from Aligned Molecules, Phys. Rev. Lett. **99**, 113901 (2007).

[26] A. Zavriyev, P. H. Bucksbaum, H. G. Muller, and D. W. Schumacher, Ionization and dissociation of H_2 in intense laser fields at 1.064 μm, 532 nm, and 355 nm, Phys. Rev. A **42**, 5500 (1990).

[27] E. E. Aubanel, J.-M. Gauthier, and A. D. Bandrauk, Molecular stabilization and angular distribution in photodissociation of H_2^+ in intense laser fields, Phys. Rev. A **48**, 2145 (1993).

[28] Y.-C. Han, K.-J. Yuan, W.-H. Hu, and S.-L. Cong, Control of photodissociation and photoionization of the NaI molecule by dynamic stark effect, J. Chem. Phys. **130**, 044308 (2009).

[29] A. Csehi, G. J. Halász, L. S. Cederbaum, and A. Vibók, Tracking the photodissociation probability of D_2^+ induced by linearly chirped laser pulses, J. Chem. Phys. **144**, 074309 (2016).

[30] A. Tóth, A. Csehi, G. J. Halász, and A. Vibók, Control of photodissociation with the dynamic stark effect induced by THz pulses, Phys. Rev. Res. **2**, 013338 (2020).

[31] Z. Chen, P.-L. He, and F. He, Spiral nuclear momentum distribution for the dissociation of ${H_2}^+$ in a circularly polarized laser pulse, Phys. Rev. A **101**, 033406 (2020).

[32] F. He, C. Ruiz, and A. Becker, Control of Electron Excitation and Localization in the Dissociation of ${H_2}^+$ and its Isotopes Using Two Sequential Ultrashort Laser Pulses, Phys. Rev. Lett. **99**, 083002 (2007).

[33] M. McDonald, B. H. McGuyer, F. Apfelbeck, C. H. Lee, I. Majewska, R. Moszynski, and T. Zelevinsky, *et al.*, Photodissociation of ultracold diatomic strontium molecules with quantum state control, Nature (London) **535**, 122 (2016).

[34] M. E. Corrales, R. de Nalda, and L. Bañares, Strong laser field control of fragment spatial distributions from a photodissociation reaction, Nat. Commun. **8**, 1345 (2017).

[35] J. Wang, Q. Meng, and Y. Mo, Oscillation of Branching Ratios Between the $D(2s) + D(1s)$ and the $D(2p) + D(1s)$ Channels in Direct Photodissociation of D_2, Phys. Rev. Lett. **119**, 053002 (2017).

[36] C.-X. Hu, W.-Z. Li, W.-B. Zhang, X.-C. Gong, J. Wu, and F. He, Angle-resolved Rabi flopping in strong-field dissociation of molecules, Phys. Rev. A **103**, 043122 (2021).

[37] Y. R. Liu, Y. Wu, J. G. Wang, O. Vendrell, V. Kimberg, and S. B. Zhang, Electron-rotation coupling in diatomics under strong-field excitation, Phys. Rev. A **102**, 033114 (2020).

[38] Y. R. Liu, Y. Wu, J. G. Wang, O. Vendrell, V. Kimberg, and S. B. Zhang, Photodissociation dynamics of the NH molecule under intense VUV pulses, Phys. Rev. Research **2**, 043348 (2020).

[39] Y. P. Zhu, Y. R. Liu, X. Zhao, V. Kimberg, and S. B. Zhang, Core-excited molecules by resonant intense x-ray pulses involving electron-rotation coupling, Chin. Phys. Lett. **38**, 053201 (2021).

[40] Y. R. Liu, V. Kimberg, Y. Wu, J. G. Wang, O. Vendrell, and S. B. Zhang, Ultraviolet pump–probe photodissociation spectroscopy of electron-rotation coupling in diatomics, J. Phys. Chem. Lett. **12**, 5534 (2021).

[41] P. Badankó, G. J. Halász, L. S. Cederbaum, A. Vibók, and A. Csehi, Communication: Substantial impact of the orientation of transition dipole moments on the dynamics of diatomics in laser fields, J. Chem. Phys. **149**, 181101 (2018).

[42] M. Aymar, R. Guérout, M. Sahlaoui, and O. Dulieu, Electronic structure of the magnesium hydride molecular ion, J. Phys. B: At. Mol. Opt. Phys. **42**, 154025 (2009).

[43] A. Bertelsen, I. S. Vogelius, S. Jørgensen, R. Kosloff, and M. Drewsen, Photo-dissociation of cold MgH^+ions, Eur. Phys. J. D **31**, 403 (2004).

[44] S. Jø rgensen, M. Drewsen, and R. Kosloff, Intensity and wavelength control of a single molecule reaction: Simulation of photodissociation of cold-trapped MgH^+, J. Chem. Phys. **123**, 094302 (2005).

[45] S. Kahra, G. Leschhorn, M. Kowalewski, A. Schiffrin, E. Bothschafter, W. Fuß, R. de Vivie-Riedle, R. Ernstorfer, F. Krausz, R. Kienberger, *et al.*, A molecular conveyor belt by controlled delivery of single molecules into ultrashort laser pulses, Nat. Phys. **8**, 238 (2012).

[46] R. N. Zare, *Angular Momentum: Understanding Spatial Aspects in Chemistry and Physics* (Wiley, New York, 1988)

[47] H. Lefebvre-Brion and R. W. Field, *The Spectra and Dynamics of Diatomic Molecules: Revised and Enlarged Edition* (Elsevier, New York, 2004).

[48] A. Tóth, A. Csehi, G. J. Halász, and A. Vibók, Photodissociation dynamics of the LiF molecule: Two- and three-state descriptions, Phys. Rev. A **99**, 043424 (2019).

[49] M. Beck, A. Jackle, G. Worth, and H.-D. Meyer, The multiconfiguration time-dependent Hartree (MCTDH) method: A highly efficient algorithm for propagating wavepackets, Phys. Rep. **324**, 1 (2000).

[50] A. Ben Haj-Yedder, A. Auger, C. M. Dion, E. Cancès, A. Keller, C. Le Bris, and O. Atabek, Numerical optimization of laser fields to control molecular orientation, Phys. Rev. A **66**, 063401 (2002).

[51] G. A. Worth, M. H. Beck, A. Jäckle, O. Vendrell, and H.-D. Meyer, The MCTDH Package, Version 8.2, (2000). H.-D. Meyer, Version 8.3 (2002), Version 8.4 (2007). O. Vendrell and H.-D. Meyer Version 8.5 (2013). Version 8.5 contains the ML-MCTDH algorithm. Current versions: 8.4.18 and 8.5.11 (2019). Used version: “Used version” See http://mctdh.uni-hd.de/.